Dynamic high-temperature crystallization and processing properties of industrial soda–lime–silica glasses

KILINC, Erhan <http://orcid.org/0000-0002-5280-0275>, BELL, Anthony <http://orcid.org/0000-0001-5038-5621> and BINGHAM, Paul <http://orcid.org/0000-0001-6017-0798>

Received: 23 June 2023 | Revised: 6 November 2023 | Accepted: 6 November 2023

DOI: 10.1111/jace.19602

Journal of the American Ceramic Society

RESEARCH ARTICLE

Dynamic high-temperature crystallization and processing properties of industrial soda–lime–silica glasses

Erhan Kilinc | **Anthony M. T. Bell** | **Paul A. Bingham**

Materials and Engineering Research Institute, College of Business, Science and Technology, Sheffield Hallam University, Sheffield, UK

Correspondence
Erhan Kilinc, Materials and Engineering Research Institute, College of Business, Science and Technology, Sheffield Hallam University, Sheffield, S1 1WB, UK.
Email: e.kilinc@shu.ac.uk

Editor's Choice
The Editor-in-Chief recommends this outstanding article

Abstract

In situ dynamic crystallization properties of industrial soda–lime–silica glasses at realistic processing temperatures have not yet been explored. Hence, we collected in situ high-temperature X-ray diffraction patterns for 10 different industrially manufactured soda–lime–silica glasses as a function of temperature between 900 and 1200°C to investigate the phase relations in their devitrified melts. The high-temperature X-ray diffraction study was complemented by measuring the liquidus temperature of those glasses by the temperature gradient technique. A multiple variable regression analysis was applied to the experimental and modeled data to produce a predictive model for the rate of solidification and liquidus temperature based on glass composition. We have demonstrated that forms of quartz (SiO_2) and Na_2CaSiO_4, which are not traditionally identified by room temperature X-ray diffraction studies of commercial soda–lime–silica glasses, are the dominant crystalline phases at 800 and 900°C. Upon further heating, different forms of cristobalite become the primary phase field prior to the formation of X-ray amorphous melts, irrespective of the glass composition. Sporadic unidentified as well as high-temperature stable SiO_2 polymorphs that are not recoverable to room temperature were also observed. In contrast to the literature, wollastonite ($CaSiO_3$) and devitrite ($Na_2Ca_3Si_6O_{16}$), which are the main predictor variables in previously developed liquidus temperature models, were not observed prior to the formation of X-ray amorphous glass melts, and hence their influence on liquidus temperature may be questionable. It was also found that the difference between glass processing and liquidus temperatures can be excessively high, and such large temperature differences can potentially be exploited and reduced to enable decreases in melting or processing temperatures of industrial soda–lime–silica glass melts.

KEYWORDS
crystals/crystallization, glass, processing, soda–lime–silica, X-ray methods

1 | INTRODUCTION

Commercial soda–lime–silica glasses such as float, container, and tableware glasses are the most common and special subtypes of silicate glasses, and their chemical compositions have evolved over time to adapt to the changing technological and processing standards on the grounds of cost and raw material availability.[1,2,3,4] These refined glass compositions[1,2] tend to reside within a specific and relatively narrow compositional range; narrower still for each glass subtype. However, workability,[5] particularly chemical durability,[6] and crystallization properties[7] of soda–lime–silica glasses can be highly susceptible to small variations in compositions.

There are small but meaningful variations between different soda–lime–silica container glass compositions; as mentioned earlier, this might be partly due to regional raw material availability.[3,8] On the other hand, refined commercial soda–lime–silica compositions tend to reside within narrow compositional region where the desired forming and melting properties are met. Moreover, compositional differences, such as variations in alkaline earth or alkali oxide concentrations can become even more distinct between float, container, and tableware processes, and such larger compositional differences would be attributed to the different constraints on which float, container, and tableware manufacturing processes are based.

Liquidus temperature is an important glass technology parameter, and it has a significant effect on the workability of commercial soda–lime–silica glasses.[9,10] Kilinc et al.[11] investigated how phase relations impact the liquidus temperature and crystallization rate of silicate glasses at a temperature that was 30°C lower than their measured liquidus temperatures. Their findings revealed that while the extent of crystallization in the glass melts may be relatively small when considering the diverse compositional modifications, there are still notable and statistically significant instances of crystal growth observed for glass melts falling within the devitrite and tridymite primary phase fields. However, when the heat treatment temperature of silicate glass melts is further reduced, it can result in significant variations in bulk crystallization and the phases that develop. Hrma et al.[7] determined liquidus temperature and the type of phase fields of the different float-type soda–lime–silica glasses and observed dramatic variations in crystallization properties within a very small compositional region at temperatures that fall into the pressing and blowing temperature range of container glasses.

The literature studies are available that link the liquidus temperature and the rate of crystallization to crystalline phase field and report that liquidus temperature and the rate of crystallization can vary dramatically depending on the type of crystal phase field in silicate glasses.[8,12,13,14] Note that X-ray diffraction or microscopy studies for determination of type of crystals were generally performed on devitrified glasses which were quenched from corresponding devitrification temperatures to room temperature.[7,15] However, crystalline phases which are identified at room temperature may not entirely represent the nature of high-temperature crystalline phases which can affect the liquidus temperature. As a result, liquidus temperature models that contain room temperature primary phase fields as input variables may lead to erroneous conclusions.

In this work, the liquidus temperature of various international container and tableware glasses were measured by conventional gradient boat method, and in situ high-temperature X-ray diffraction (HTXRD) was used to analyze the phase transformation of the studied glasses as a function of temperature. Further to this, multiple variable regression was used to develop a model that predicts the liquidus temperature of soda–lime–silica glasses based on compositions of the studied and literature glasses, and the calculated liquidus temperatures from Karlsson,[12] Fluegel,[16] Cuartas,[17] and our models were compared with some independent experimental data from the literature to test their predictive ability. The Fluegel[18] viscosity model, together with multiple variable regressions, was also used to develop a relationship between glass composition and the rate of solidification to better understand the compositional dependence of workability in soda–lime–silica glasses. We also compared the high-temperature crystalline phase fields of studied glasses with data acquired through room-temperature X-ray diffraction studies from the literature.

2 | EXPERIMENTAL PROCEDURE

2.1 | Chemical analysis of studied glasses

Six industrially manufactured containers (C-group) and four tableware glasses (T-group) are obtained from 10 different global manufacturers. Crushed glass was rinsed with distilled water and then rinsed thoroughly with acetone. Cleaned glass was ground at a rotation speed of 700 rpm for 40 s in an automated stainless steel mortar (Retsch 200), and 1 g of powdered glass was mixed with 10 g of 0.5 wt.% lithium iodide (LiI) doped lithium tetraborate ($Li_2B_4O_7$) flux, and fused beads were prepared with Claisse LeNeo Fluxer following the methodology given in the study by Bell et al.[19] and were sent to Glass Technology Services Ltd. for XRF-OXI compositional analysis. Estimated measurement uncertainty for each major oxide which may range between 65 and 77 wt.% is ±0.5 wt.%, ±0.15 wt.% for the levels of each oxide between 17 and 12 wt.%, ±0.12 wt.% for the oxides where the content of each

was between 12 and 6 wt.%, and ±0.1 wt.% for the content of each oxide less than 6 wt.%.

2.2 | Liquidus temperature measurement

The liquidus temperature can be defined as the highest temperature at which thermodynamic equilibrium coexists between the glass and the primary crystalline phase.[20,21] In this study, the temperature at which the first crystal grain starts to grow stably is referred to as the liquidus temperature when the glass is exposed to a known temperature gradient for an extended period, which is at least 24 h. The gradient boat method was applied to measure the liquidus temperature of studied glasses, and crushed glass samples were loaded into Almath BS91 alumina boats and heated from room temperature to ~1200°C to obtain glassy phase across the boat and then cooled down to the point where the specified temperature gradient is formed along the entire length of boat. It was observed that 24 and 48 h of heat treatment in a known temperature gradient was not sufficient to devitrify some of the studied C and T-group glasses, and therefore the duration of the heat treatment for all studied glass samples was extended to 168 h to enable the observation of crystals under optical microscopy, and the heat-treated glass samples were air-quenched to cool down to room temperature and the location of the crystal growth in bulky glass along the boat was examined under the microscope. The average deviation between duplicate measurements carried out under identical conditions is a maximum of 5°C, and this indicates relatively high degree of measurement repeatability. However, the estimated error for the liquidus temperature measurements tends to be larger for the studied glasses as their onset of devitrification in most cases falls within a zone where the temperature gradient in the tube furnace is relatively high (>15°C/cm), and thus the uncertainty associated with these measurements is conservatively specified as ±20°C.

2.3 | X-ray diffraction analysis

2.3.1 | High-temperature X-ray powder diffraction data collection

Each sample (0.16 g of glass) was loaded into a platinum flat plate sample holder and mounted onto the Anton Paar HTK1200N high-temperature stage. High-temperature X-ray powder diffraction data were collected on the PANalytical X'Pert X-ray powder diffractometer. Data were collected using CuKα X-rays using the PIXCEL-1D multichannel detector over the range 10°–80° 2θ, each diffraction scan took 30 min.

For each sample, an initial 30-min room temperature scan was done before the sample heating started. The sample was heated to 800°C at a heating rate of 10°C/min; and a high number of XRD scans (30 × 30-min scans) were applied to closely monitor how the crystalline phases form, disappear, or remain stable at 800°C and other heat treatment stages. The sample again was heated to 900°C at a ramp rate of 10°C/min then 30 × 30-min scans were done at 900°C. Finally, the sample was heated up to 1200°C at a heating rate of 1°C/min, and single 30 min scans were done every 5°C from 905 to 1200°C. The total heat treatment duration for the studied glasses was 65 h and 10 min, but this duration excludes the initial time spent rapidly heating up the HTXRD stage to 800°C.

In each case, the sample was amorphous at room temperature, there were two broad weak peaks in the XRD data around 14 and 18° 2θ, these were due to scatter from the window material of the high-temperature stage.

For each glass sample, the initial amorphous XRD patterns would start to incorporate more and more Bragg peaks as the glass started to devitrify and become crystalline. In the highest temperature scans, done over the temperature range 905–1200°C, the Bragg peaks would start to fade away with increasing temperature until all the Bragg peaks disappeared as the sample had completely melted. In some cases, Bragg peaks due to platinum, from the sample holder, were also seen in the XRD patterns. The PANalytical HighScore Plus software, together with the ICDD powder diffraction file (PDF) was then used to analyze these high-temperature XRD data.

2.3.2 | Room temperature X-ray powder diffraction collection

At least 7.0 g C_3 glass was placed into an Au-stabilized Pt crucible and heated to ~30°C below its actual liquidus temperature of 1063°C, at a heating rate of 10°C/min and maintained at this temperature for 48 h to grow crystalline phases and identify them by X-ray powder diffraction. Following, devitrified C_3 glass was air-quenched to room temperature. Devitrified glass sample was then removed from the crucible and ground for 60 s with a rotation rate of 700 rpm in an automated stainless-steel mortar. Powdered devitrified C_3 glass was loaded into a flat plate sample holder for X-ray Powder Diffraction. XRD data were collected using the PANalytical X'Pert Pro MPD X-ray powder diffractometer. Cu K-alpha X-rays were used and the sample was rotated once every 4 s. Room-temperature XRD data were collected over the range of 10° to 80° 2θ and the total measuring time was 16 h. Analysis of the XRD data was performed using HighScore Plus (PANalytical) and the ICDD PDF.

2.4 | Determination of degree of volatilization during heat treatment

As stated in Sections 2.2 and 2.3, the total heat treatment duration for the studied glasses during the liquidus temperature and HTXRD experiments was 168 h and 65 h 10 min, respectively. In order to assess the degree of potential alkali volatilization from the melts during these extended experiments, we simulated both HTXRD and liquidus temperature experiments at various temperatures and durations using the representative C_3 glass. Approximately 8 to 10 g of a C_3 glass fragment was used for each extended heat treatment. The first C_3 glass sample was subjected to the heat treatment temperature of 1033°C for a duration of 48 h, and the second C_3 glass specimen was exposed to the heat treatment temperature of 1090°C for 168 h, both in Au-stabilized Pt crucibles using a heating rate 10°C/min. Then, the chemical compositions of both heat-treated and untreated (as-received) glasses, with particular attention to Na_2O and K_2O concentrations, were measured with an in-house quantitative New-OXI XRF by following the fused bead preparation method given in Section 2.1. These experiments were performed because any significant differences in Na_2O and K_2O concentrations may indicate changes in the bulk glass composition due to volatilization during the HTXRD and liquidus temperature experiments.

2.5 | Viscosity and liquidus temperature modeling

Various models have been developed to describe the temperature—viscosity relationship of both organic and inorganic liquids, including silicate glasses. For instance, the Adam– Gibbs (AG), Avramov—Milchev (AM), Mauro–Yue– Ellison—Gupta—Allan (MYEGA), and Vogel—Fulcher—Tammann (VFT) equations aim to predict the viscosity of glass at different temperatures and are used to understand its behavior during different stages of glass processing.[22] The VFT equation is one of the simplest[23] and most widely used models to describe the temperature dependence of the viscosity of glass-forming liquids. However, the VFT model may present limitations and less accurate fits with experimental data at low viscosities ($\eta < 10^3$ dPa·s) for fully depolymerized melts,[24] and the high-temperature viscosity of inorganic glasses can be well presented by the Arrhenius equation.[25] We note that the Arrhenius equation breaks down predicting the viscosity values of commercial glasses at temperatures lower than 1000°C, and this nearly corresponds to the viscosity value of 10^4 dPa·s for most commercial soda–lime–silica glasses.[25]

Fluegel[18] developed a model using a global statistical approach based on a dataset of more than 2200 silicate glass composition–viscosity data, including commercial container and float glasses, from scientific literature; therefore, this model correlates VFT constants directly to silicate glass compositions. Nevertheless, we used the Fluegel viscosity model to fit the experimental viscosity dataset from Bingham and Marshall[10] to evaluate how accurately this model can predict viscosity under high-temperature conditions for theoretical glass compositions compositionally similar to the glasses studied here. We obtained that the mean delta value with standard deviation (σ) for the various delta values between the experimental and predicted temperatures for nine glasses at Log (η/dPa·s) = 2, 3, and 4 was 6.7°C ($\sigma = \pm$ 9.1), −5.9°C ($\sigma = \pm$ 8.1), and −6.5°C ($\sigma = \pm$ 5.1), respectively. This shows that the Fluegel viscosity model presents reasonably good predictive power for these glasses in the high temperature regions. However, the predicted temperatures for two B_2O_3-containing glasses demonstrate a relatively higher deviation from experimentally obtained temperatures, leading to a larger standard deviation for the mean of the delta temperatures in the dataset. The exclusion of B_2O_3-containing glasses from the modeled dataset reduces the mean delta and σ of the delta values between experimental and predicted temperatures particularly at log (η/dPa·s) = 2. The mean delta and σ of these delta values between experimental and predicted temperatures for non-B_2O_3 containing soda–lime–silica glasses are 3.2°C ($\sigma = \pm$ 5.9), −6.5°C ($\sigma = \pm$ 8.5), and −6.7°C ($\sigma = \pm$ 4.8) at log (η/dPa·s) = 2, 3, and 4, respectively.

On the other hand, Mauro et al.[22] calculated the errors associated with AM, VFT, and MYEGA models, and observed that VFT models perform poorly with high-fragility liquidus, but VFT seems to perform reasonably well for predicting viscosities of low-fragility melts such as commercial soda–lime–silica glasses. They fitted AM, VFT, and MYEGA viscosity models to high-temperature experimental viscosity data of 85 Corning glass compositions including their softening points ($10^{7.6}$ dPa·s), and the models were then extrapolated to predict 10^{12} dPa·s isokom temperature, and the calculated average error of the isokom temperature for VFT, AM, and MYEGA was 9.4, −5.6, and −0.5 K, respectively. It appears that an error of 9.4 K for the VFT model can be regarded as still acceptable, particularly when dealing with very high-viscosity regions. Nevertheless, here we have restricted the modeling of the compositional dependence of viscosity using the Fluegel viscosity model specifically to viscosities lower than log (η/dPa·s) = 7.6.

The Vogel–Fulcher–Tammann equation was used to model high-temperature viscosity of the studied glasses using the constants of A, B, and C obtained from the

Fluegel viscosity model.[18] The first derivative of Equation (1) gives rise to the rate of solidification of glass melt upon cooling[26]:

$$\text{Log}\ (\eta) = A + \frac{B}{(T - C)}, \tag{1}$$

$$\frac{d\,(\text{Log}\eta)}{dT} = -\frac{B}{(T - C)^2}, \tag{2}$$

where η is dPa·s, and T is in °C.

The constant B is intrinsic to a glass composition and network dimensionality,[27] and the value of B tends to be smaller for "long" glass melts that exhibit lower rate of solidification or a smaller change in viscosity as temperature decreases.[25] Calculated B values from the VFT equation can be used to assess the isothermal workability of glass melts, and higher B values are associated with higher relaxation moduli and low high-temperature fracture strength.[27] Further to these, the rate of solidification can also be used in place of empirical correlation of relative machine speed (relative forming speed) which was earlier developed to predict the rate of cooling of glass melts for industrial forming operations.[1,26] In this work, glass melt temperatures of 1450 and 1150°C were chosen to represent the approximate temperatures of stages of glass melt processing from refining to gob forming, respectively. According to McGraw,[28] the exterior surface of container glass cools to near temperatures 680 to 730°C during the pressing period; and therefore, a temperature of 720°C has been chosen to represent the lower temperature limit of forming process for the studied glasses here.

For a given temperature, stepwise multiple linear regression analysis was used to obtain the correlation between the rate of solidification or liquidus temperature of glasses and composition. Regression analysis is started with all candidate glass oxides and those that have p values greater than .05 are deemed to be insignificant in the model and removed, and this loop is continued until the model has the oxides that have a significant impact on the dependent variable. Further to this, we attempted to verify our developed liquidus temperature models as well as Karlsson,[12] Fluegel,[16] and Cuartas[17] models with experimental data of some independent glasses from literature.

3 | RESULTS AND DISCUSSION

3.1 | Glass composition

XRF analysis did not detect the presence of SO_3 in most of the studied commercial glasses, as demonstrated in Table 1. However, sodium sulfate or other sulfur trioxide bearing raw materials are widely used in commercial soda–lime–silica batches to adjust the batch redox number and color of soda–lime–silica glass melts.[10] SO_3-bearing raw materials decompose during batch-to-melt conversion, and much of the batched sulfur escapes by self-generating SO_2 from silicate glass melts.[1] Some of the sulfur is retained in the glass structure in the form of dissolved SO_3 and its concentration generally varies between 0.05 and 0.3 wt.% in commercial soda–lime–silica glasses depending on the color and redox properties of the melts.[2,29] However, sulfate volatilization has been well-documented in X-ray fluorescence fused bead preparation,[19] and this suggest that the retained SO_3 in most studied glasses were lost completely through volatilization during fusion bead process.[19] The reported lowest concentration of Fe_2O_3 that can be detected in soda–lime–silica glasses using quantitative XRF analysis from a fused bead is ~0.03 wt. %.[30] However, it should be noted that iron oxide concentrations are typically restricted to levels smaller than 0.025 wt.% in T-group glasses as the higher levels of iron oxide can have a detrimental effect on the optical properties of T-group glasses.[1] Therefore, very small Fe_2O_3 levels in the studied T-group glasses may not be detected by XRF analysis using the fusion method, as shown in Table 1. In addition, green and amber glass compositions include significant amounts of Fe_2O_3 and FeO ranging between 0.09 and 0.6 wt.%, and Cr_2O_3 is also found in green glass compositions ranging from 0.1 to 0.3 wt.%.

(SiO_2+Al_2O_3) concentrations of the studied glasses and their mean values for T- and C-group glasses do not differ from each other significantly, as shown in Table 2 and Figure 1A,B. These specific total-network forming oxide levels may be regarded as optimal for glass processing parameters by glass manufacturers. Note that SiO_2 concentration in the studied glasses exhibits a relatively wider range, varying from approximately 70.33 to 73.09 wt.% (Table 1). Despite this, adjustments are made to the levels of Al_2O_3 to maintain the total concentration of network-forming oxides at these specific levels. On the other hand, Na_2O concentrations of T-group glasses tend to be significantly larger than those of C-group glasses. MgO concentrations of T-group glasses vary within a relatively wider range than that of C-group glasses, and most C-group glasses contain larger amounts of CaO than those of T-group glasses. Further to this, K_2O appears to be present at significant levels in C-group glasses, and this might be due to the use of K_2O-bearing feldspathic minerals as a source of Al_2O_3 where sodium feldspar is unavailable; or K_2O might be added deliberately to improve chemical durability of C-group glasses through mixed-alkali effect.[31] Overall, the mean values of total alkali and alkaline earth oxide concentrations in the T- and C-group glasses present significant variations from each other, as is seen from Figure 1B. Specifically, the T-group glasses exhibit significantly higher total alkali oxide and lower alkaline earth oxide concentrations compared with the C-group glasses.

TABLE 1 The chemical compositions of the as-produced studied glasses measured by XRF at Glass Technology Service, UK.

Glass Code	SiO_2	Na_2O	CaO	MgO	Al_2O_3	K_2O	SO_3	Cr_2O_3	Fe_2O_3	Total
T_1	71.87	14.62	10.69	0.92	1.45	0.20	0.26	0.000	0.000	100
T_2	73.09	13.72	9.05	2.82	1.07	0.26	0.00	0.000	0.000	100
T_3	72.52	13.33	11.28	1.34	1.52	0.00	0.00	0.000	0.000	100
T_4	71.74	14.74	8.74	3.33	1.45	0.00	0.00	0.000	0.000	100
C_1	72.01	11.80	10.29	2.07	2.17	1.40	0.15	0.015	0.092	100
C_2	72.85	11.90	10.95	1.80	1.32	0.52	0.00	0.244	0.426	100
C_3	72.15	12.11	11.48	1.41	1.53	0.73	0.00	0.000	0.590	100
C_4	70.33	13.67	10.64	2.83	1.90	0.00	0.00	0.299	0.326	100
C_5	72.88	12.56	10.81	2.00	1.21	0.54	0.00	0.000	0.000	100
C_6	71.87	12.80	11.16	1.58	1.53	1.07	0.00	0.000	0.000	100

Note: C_1 glass is half-white, C_2 and C_4 glasses are green, and C_3 glass is amber container glass. Oxide concentrations are in wt.%.

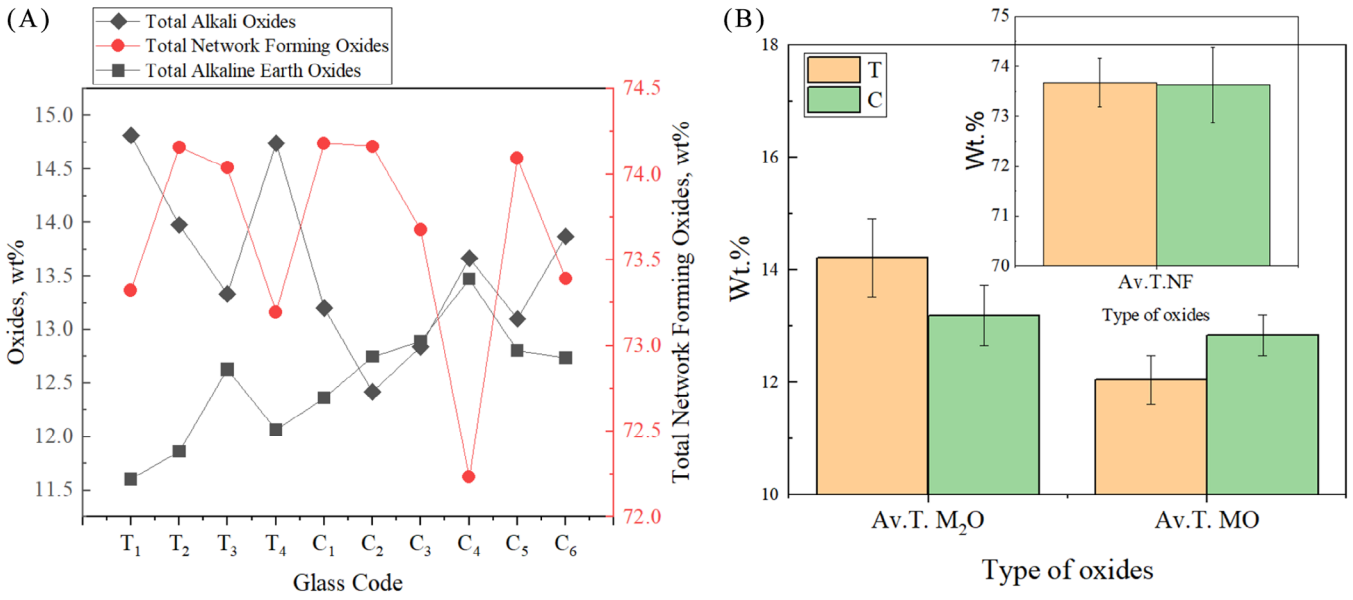

FIGURE 1 (A) Total alkali, alkaline–earth, and network-forming oxide concentrations of studied T- and C-group glasses. (B) The mean values of total alkaline earth (MO), alkali (M_2O), and network former (NF) oxide concentrations of glasses in T- and C-group glasses.

The average composition of eighteen industrially produced float glasses (in wt.%) that are taken from the work of Sinton and LaCourse[6] is 72.33·SiO_2, 0.96·Al_2O_3, 14.16·Na_2O, 0.22·K_2O, 3.33·MgO, 8.73·CaO, and 0.28·Fe_2O_3; and this indicates that Al_2O_3 content of C- and T-group glasses significantly greater than that of commercial float glasses. However, MgO and SiO_2 contents of float glasses tend to be larger than that of C-group glasses, but most T-group glass compositions resemble float glass compositions closely as their MgO and CaO contents vary within a similar range. The lowest total alkali oxide levels (Na_2O+K_2O) are observed for C_2 and C_3 glasses (Table 2), and these concentrations are considerably low levels for even container glass manufacturing. Note that C-group glasses also contain the largest amount of alkaline earth oxides (MgO+CaO) in contrast to the levels observed in T-group glasses. It appears that there is inverse variation between total alkali and total network forming oxide (SiO_2+Al_2O_3) levels in T- and C-group glasses (Figure 1A); this trend suggests that soda–lime–silica glasses which are low in alkali oxide tend to be richer in SiO_2 or Al_2O_3. It appears that container glass compositions have been adapted to high-forming speed IS machines, and this can be generally achieved by lowering alkali oxide and increasing alkaline earth oxide concentrations in container glass compositions.[32,33] However, increasing CaO and decreasing alkali oxide concentrations can increase the rate of crystallization and liquidus temperature of soda–lime–silica glasses,[8,34] but deterioration in crystallization properties can be mitigated through careful adjustments to the balance of Al_2O_3, MgO, and SiO_2 in the glass composition.[11]

TABLE 2 Total alkali (Na_2O+K_2O), alkaline earth (CaO+MgO), and network former ($SiO_2+Al_2O_3$) oxide concentrations of each studied glasses, and the mean values of total alkali, alkaline earth, and network former oxide concentrations of glasses in T- and C-group glasses.

Glass code	Total alkali oxide	Total alkaline earth oxide	Total network formers
T_1	14.81	11.61	73.32
T_2	13.98	11.86	74.16
T_3	13.33	12.63	74.04
T_4	14.74	12.07	73.20
C_1	13.20	12.36	74.18
C_2	12.42	12.75	74.16
C_3	12.84	12.89	73.68
C_4	13.67	13.47	72.23
C_5	13.10	12.81	74.09
C_6	13.87	12.74	73.39
Glass group	**Mean of total alkali oxide**	**Mean of total alkaline earth oxide**	**Mean of total network formers**
T	14.22 ± 0.70	12.04 ± 0.43	73.68 ± 0.49
C	13.18 ± 0.53	12.84 ± 0.36	73.62 ± 0.75

Note: Oxide concentrations are in wt.%.

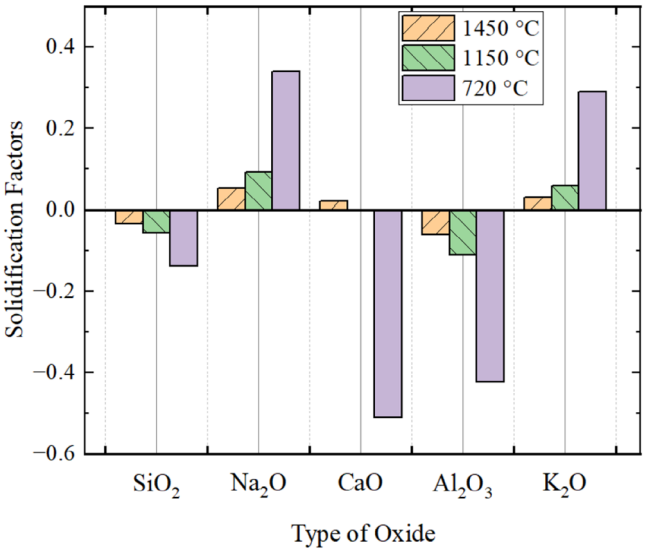

FIGURE 2 Solidification factors of studied T- and C-group glasses obtained from multiple variable regression analysis. Solidification factors define the regression coefficients, which indicate the extent to which the independent variables or oxides affect the ROS.

3.2 | Rate of solidification of melts

The rate of solidification (ROS) is defined by Equation (2), and the predictive models for the rate of solidification (ROS_{1450}, ROS_{1150}, and ROS_{720}) of soda–lime–silica glass melts as a function of glass composition at temperatures of 1450, 1150, and 720°C were presented in the form of Equations (3), (4), and (5). The chemical formulas stand for the mass percentage of oxides that are considered significant contributors to the model's prediction of ROS. The first coefficients or the constant terms in Equations (3), (4), and (5) are the y-intercepts produced by the multiple regression analysis.

$$ROS_{1450} = -1.477 - 0.034\,[SiO_2] + 0.053\,[Na_2O] + 0.021\,[CaO] - 0.061\,[Al_2O_3] + 0.030\,[K_2O], \quad (3)$$

$$ROS_{1150} = -2.562 - 0.056\,[SiO_2] + 0.094\,[Na_2O] - 0.111\,[Al_2O_3] + 0.058\,[K_2O], \quad (4)$$

$$ROS_{720} = -9.550 - 0.139\,[SiO_2] + 0.340\,[Na_2O] - 0.512\,[CaO] - 0.424\,[Al_2O_3] + 0.290\,[K_2O]. \quad (5)$$

Equation (3) defines the ROS of soda–lime–silica glass melts at high-temperature regions, and ROS near melting or refining temperatures can be correlated to the levels of SiO_2, Al_2O_3, Na_2O, and CaO. The negative coefficients for SiO_2 and Al_2O_3 define that these oxides increase the rate of solidification, whereas the positive coefficients for Na_2O, K_2O, and CaO indicate that these oxides decrease the rate of solidification of silicate melts during cooling. It appears that Al_2O_3 and Na_2O have the strongest effect in increasing and decreasing the solidification rate of melts near melting and conditioning temperatures, respectively.

However, as shown in Figure 2, the role of oxides on the rate of solidification tends to differ throughout the entire temperature–viscosity curve. SiO_2 and Al_2O_3 as network formers and Na_2O and K_2O as network modifiers exhibit statistically significant roles in the rate of solidification of glass melts near forming temperatures, and Equation (4) demonstrates that Al_2O_3 and Na_2O are the main oxides which mainly govern the rate of solidification near at gob forming or conditioning temperatures.

Equation (5) suggests that CaO and Al_2O_3 strongly reduce the cooling time of soda–lime–silica glass melts as they significantly raise the solidification rate of the silicate melts near at forming temperature region. Equations (3), (4), and (5) also indicate that there is not a statistically significant correlation between the solidification rate of melts and MgO at high- and low-temperature regions. It is well known that Al_2O_3 strongly increases the viscosity of industrial glass melts, but the effect is more obvious at low temperatures.[18] The experimental work of Xiao et al.[35] also confirms our modeled properties that the addition of Al_2O_3 in place of SiO_2 gives rise to steeper solidification rates that may deteriorate processing and forming properties of the melt in the float chamber. Second, float glass does not necessarily have to be highly resistant to water and chemical attacks in comparison to container and

TABLE 3 Modeled working properties of the T- and C-group glasses.

Properties	Glass codes									
	T_1	T_2	T_3	T_4	C_1	C_2	C_3	C_4	C_5	C_6
Log2	1430.20	1458.30	1452.20	1441.40	1473.00	1471.70	1459.80	1437.40	1460.60	1447.70
Log3	1176.70	1198.90	1195.70	1184.50	1213.60	1212.20	1202.10	1183.10	1202.70	1191.40
Log4	1014.10	1031.20	1031.10	1018.70	1045.80	1045.00	1036.70	1020.00	1036.70	1027.10
Log7.6	722.60	727.30	735.70	719.20	741.90	743.10	739.60	727.20	737.30	732.20
A	−2.57	−2.66	−2.58	−2.64	−2.66	−2.63	−2.58	−2.58	−2.62	−2.57
B	4137.95	4423.67	4200.24	4331.40	4421.65	4351.12	4229.90	4162.03	4304.93	4185.27
T	271.34	249.52	278.00	250.19	264.34	271.48	278.98	273.59	270.21	275.93
T_L	1025	947	1053	961	1025	1049	1063	1032	1057	1020
T_{3G}-T_L	211.70	251.90	142.70	223.50	188.60	163.20	139.10	151.10	145.70	171.40

Note: *A*, *B*, and *T* are the coefficients from fitting Equation (1) to data. Temperatures at corresponding Logη viscosity (dPa·s) is in °C.

domestic glass, and therefore the Al_2O_3 content of most float glasses tends to be lower than that of container and domestic glasses. Whereas Al_2O_3 significantly improves the workability of silicate glass melts as its presence even at small amounts dramatically reduces liquidus temperature of silicate glass melts.[11] In contrast to the role of CaO, SiO_2, and Al_2O_3; alkali oxides (Na_2O and K_2O) tend to reduce the rate of solidification with positive coefficients.

3.3 | Liquidus temperature and workability

The viscosity range for producing gobs for commercial container glass is reported[9] to be between $10^{3.5}$ and $10^{3.7}$ dPa·s. However, viscosity in this range may be regarded as relatively high as the modern individual section (IS) machines require glass gobs with relatively lower viscosity to ensure faster gob delivery speeds. The typical viscosity which may be optimal for achieving faster gob delivery speeds is around 10^3 dPa·s for modern container glass compositions studied here.[32] In this work, T_{3G} stands for the temperature at which the ideal viscosity of 10^3 dPa·s is attained for producing optimum container glass gob for the studied glasses. The delta between gob and liquidus temperatures (T_{3G}—T_L) provides valuable information in assessing the practicality of working with reformulated or newly designed glass compositions.[11] Positive sign of delta can be related to better workability properties as such positive variation in delta reduces the likelihood of devitrification product formation not only in forehearths but also at the melting tank bottom where the glass melt temperatures can be approximately 200°C lower than the furnace hot spot.[36] On the other hand, the delta between gob and liquidus temperature for T- and C-group glasses (Table 3)—that is, ~251°C and 188°C for T_2 and C_1 glass, respectively—appears to be very conservative and high, and this might enable technologists to further optimize and reduce melting and conditioning temperatures to reduce energy consumption, CO_2 footprint, and refractory corrosion rates. Note that delta between T_{3G} and T_L for T-group glasses is much more pronounced than that of C-group glasses, and this can be attributed to considerably low liquidus temperatures of T-group glasses.

The relationship between glass composition and liquidus temperature is not clear-cut and can be often described as nonlinear,[37,38,39] and there can be a large discrepancy between modeled and actual liquidus temperatures for glass compositions that reside in between different phase fields.[39] Hrma et al.[7] studied the phase fields and liquidus temperature of float-like soda–lime–silica glasses, and these glasses were found to have liquidus temperatures similar to those seen in T-group glasses but much lower than those found in C-group glasses. Moreover, liquidus temperature of the glasses studied by Hrma et al.[7] varied significantly, ranging from 1040 to 980°C, even within a slightly modified compositional range.

The multiple regression models (see Equations (6) and (7)), which were developed by collating the liquidus temperatures of T, C-group, and literature glasses[7,11] (Table 4), demonstrate that SiO_2, Al_2O_3, MgO, and CaO are the main oxides governing liquidus temperature of soda–lime–silica glasses, but the effect of CaO and MgO appears to be more pronounced than that of SiO_2 and Al_2O_3 in increasing the liquidus temperatures. The first coefficients or the constant terms in Equations (6) and (7) are the y-intercepts, and they are the output of the multiple regression analysis. The regression analysis indicates that the *p*-values associated with the Na_2O and K_2O variables are greater than .05, and this suggests that these variables are not statistically significant contributors to the model's prediction of liquidus temperature, and they were removed from initial regression analysis, and the following predictive model for liquidus temperature (TL1) was developed. The chemical formulas stand for the mass percentage of oxides that are considered significant contributors to the model's

TABLE 4 Glass compositions (wt.%) from the literature that are used to develop our liquidus temperature model.

Glass ID	SiO_2	Al_2O_3	Na_2O	MgO	CaO	Fe_2O_3	K_2O	T_L/°C
A-BL	73.18	0.45	13.63	3.47	8.45	0.71	0.1	995
A-LNA	73.68	0.45	13.13	3.47	8.45	0.71	0.1	1011
A-HNA	72.68	0.45	14.13	3.47	8.45	0.71	0.1	989
A-LCA	73.68	0.45	13.63	3.47	7.95	0.71	0.1	993
A-HCA	72.68	0.45	13.63	3.47	8.95	0.71	0.1	1011
A-LMG	73.68	0.45	13.63	2.97	8.45	0.71	0.1	997
A-HMG	72.68	0.45	13.63	3.97	8.45	0.71	0.1	1001
B-BL	73.53	0.1	13.7	3.47	8.45	0.71	0.03	997
B-LNA	74.03	0.1	13.2	3.47	8.45	0.71	0.03	1044
B-HNA	73.03	0.1	14.2	3.47	8.45	0.71	0.03	980
B-LCA	74.03	0.1	13.7	3.47	7.95	0.71	0.03	1024
B-HCA	73.03	0.1	13.7	3.47	8.95	0.71	0.03	1001
B-LMG	74.03	0.1	13.7	2.97	8.45	0.71	0.03	1026
B-HMG	73.03	0.1	13.7	3.97	8.45	0.71	0.03	995
C-HAI	73.34	0.45	13.15	3.47	8.45	0.71	0.08	1017
C-MAI	72.53	0.25	13.79	3.67	8.65	0.71	0.04	1000
C-LAI	72.31	0.06	13.83	3.87	8.85	0.71	0	1002
M_2S_{73}	72.85	2.51	13.7	1.26	9.58	0.11	0	1022
M_3S_{72}	72.31	2.58	13.31	2	9.72	0.08	0	1045
M_4S_{71}	71.07	2.59	13.93	2.58	9.75	0.08	0	1030
M_5S_{70}	70.15	2.58	14.29	3.26	9.62	0.11	0	1049
M_6S_{69}	69.69	2.64	13.91	3.93	9.75	0.08	0	1046
C_9S_{73}	73.16	2.62	13.51	1.93	8.7	0.08	0	1000
$C_{11}S_{71}$	71.17	2.57	13.5	1.99	10.69	0.08	0	1036
$C_{12}S_{70}$	70.36	2.54	13.6	1.93	11.49	0.08	0	1073
M_1C_{12}	71.93	2.13	13.9	0.67	11.3	0.08	0	1045
M_5C_8	73.35	2.02	13.59	3.22	7.72	0.11	0	976

Note: Glasses from A-BL to C-LAI are taken from the study by Hrma et al.[7]; and glasses from M_2S_{73} to M_5C_8 are taken from the study by Kilinc et al11.

prediction of liquidus temperatures.

$$TL\,(1) = -1607 + 27.978\,[SiO_2] + 26.918\,[Al_2O_3] + 42.858\,[MgO] + 47.132\,[CaO]\,. \quad (6)$$

The fact that the impact of alkali oxides, particularly Na_2O, on crystalline phase fields and liquidus temperature is well-established in the traditionally ternary Na_2O–CaO–SiO_2 diagram[40] and has been included as a variable in previous liquidus temperature models by Fluegel, Karlsson, and Cuartas further justifies its addition in our analysis. Hence, we have decided to introduce Na_2O as a variable in an alternative predictive model (see Equation (7)) for liquidus temperature (TL2) to assess its impact on the model strength without using the traditional *p*-value criterion.

$$TL\,(2) = -1641 + 28.329\,[SiO_2] + 0.307\,[Na_2O] + 47.528\,[CaO] + 27.153\,[Al_2O_3] + 43.231\,[MgO]\,. \quad (7)$$

It was previously shown that Fluegel's liquidus temperature model[16] provides a good fit to the experimental liquidus temperature data of various soda–lime–silica glasses measured by gradient boat method.[11] Here commercial container and float glass compositions from the literature were used to assess the performance of our own developed TL(1) and TL(2) models, as well as the Fluegel, Karlsson, and Cuartas liquidus temperature models. Note that liquidus temperature can be influenced by the experimental procedure in practice, and each literature float glass obtained from the study by Beerkens and Conradt[15] (F_1, F_2, and F_3) has different liquidus temperature values measured by different techniques. Hence, we considered the liquidus temperatures that were measured by the gradient boat method consistent with our and other (K, L, and M) literature glasses.[10] Table 5 indicates that our developed models (TL1 and TL2) as well as Fluegel, Karlsson, and Cuartas liquidus models provide a good and similar predictive accuracy. Interestingly the comparison table also

TABLE 5 Comparison between different liquidus temperature models with respect to measured liquidus temperature of selected literature glasses.

	Bingham and Marshall, 2005			Beerkens and Conradt, 2008		
	K	***L***	***M***	***F1***	***F2***	***F3/F6***
SiO_2	72.5	71.1	70.2	72.6	72.6	72
Na_2O	13.3	14.6	13.3	13.5	14	13.5
K_2O	0.4	0.4	2.5	0.2	0	0.7
MgO	1.7	1.6	1.7	4.4	4.1	4
CaO	10.6	10.8	10.7	8.4	8.8	8.5
Al_2O_3	1.2	1.2	1.1	0.5	0.1	1.1
Fe_2O_3	0	0	0	0.1	0.1	0.1
SO_3	0.3	0.3	0.3	0.2	0.2	0.2
TiO_2	0	0	0	0.2	0	0
Actual liquidus T/°C	1015	1010	990	1003.5	1004.5	1007.5
Our TL (1) model/°C	1026	992	964	1022	1017	1009
Our TL (2) model/°C	1026	992	963	1022	1018	1009
Fluegel's model/°C	1036	1040	1052[a]	995	995	1007
Karlsson's model/°C	1037	1028	1007	1000	941[a]	1010
Cuartas' model/°C	1066[a]	1031	1014	1025	1011	1026

Note: Oxide concentrations are in wt.%.

[a]Significantly large temperature difference between modeled and experimental data.

displays that the presence or absence of Na_2O as a variable in the developed models does not significantly alter the strength of the predictive models (Equations (6) and (7)). However, occasional significantly large deviations, greater than 50°C, between predicted and experimental values were observed (see Table 5) when Fluegel, Karlsson, and Cuartas liquidus models were used. Note that the number of data set that was used to validate these models are low, and the accuracy of the model verification can be increased by adding more independent and qualified experimental data sets that were not previously used in the estimation of model parameters.

3.3.1 | Effect of alkali volatilization on liquidus temperature

Our XRF analysis shows that the Na_2O concentration for the heat-treated C_3 glass at 1033°C for 48 h, and at 1090°C for 168 h, and for the as-received C_3 glass were 12.03, 12.12, and 12.23 wt.%, respectively, with a standard deviation of ±0.03 wt.%. Similarly, the K_2O concentration for the heat-treated C_3 glasses at 1033 and 1090°C, and for the as-received C_3 glass were 0.71, 0.69, and 0.70 wt.%, respectively. These findings suggest that the differences in alkali oxide concentrations, particularly for Na_2O, between the 48 and 168 h heat-treated and as-received C_3 glasses are small and therefore do not indicate any significant levels of alkali volatilization which, if present, may have impacted the liquidus temperature or the type of the crystalline phase fields of bulk T- and C-group glasses observed during the liquidus temperature and HTXRD experiments. Consequently, the possibility of any significant levels of alkali volatilization from the interior (bulk) T- and C-group glasses during the extended experiments can be discounted. However, XRF analysis of the heat-treated bulk glass samples may not accurately represent the composition of an alkali-depleted thin surface layer that could form during an extended period of heat treatment[41,42] as this thin surface layer may not measurably influence the overall or bulk glass composition. On the other hand, the calculated equilibrium constants of sodium evaporation reactions (specifically the formation reaction of NaOH) from silicate glasses were 7.16×10^{-2} and 4.17 at 1000 and 1400°C, respectively.[41] Beerkens[42] similarly noted that sodium volatilization reaction kinetics at 1500°C are at least two orders of magnitude higher than at 1000°C. This suggests that whilst some level of alkali volatilization will have occurred during the extended experiments in the present study, the degree of volatilization should be minimal because the rate of sodium evaporation from silicate melts at the temperatures at which the extended experiments were conducted is orders of magnitude smaller than that at higher melting temperatures. At the liquidus temperature position, our microscopic examination of the C_3 glass in the liquidus boat showed that columnar and bladed structured wollastonite-2M crystals exhibited no change in their structural characteristics in the bulk of glass, on the surface of the glass melt and at the interface between the glass and the boat. This observation is

TABLE 6 Identified crystalline phase fields of T-group glasses at 800 and 900°C and just below their HTXRD crystal dissolution points obtained by in situ HTXRD analysis.

	Type of phase fields			
Glass code	**800°C**	**900°C**	**Just below HTXRD crystal dissolution temperature**	
T_1	β-Quartz, α-quartz, β-cristobalite	Na_2CaSiO_4, β-quartz, α-quartz	α-Quartz, β-quartz	1000–1005°C
T_2	β-Quartz, β-cristobalite, α-quartz, tridymite	β-Cristobalite, α-quartz	β-Cristobalite	985–1005°C
T_3	β-Quartz, α-quartz, β-cristobalite, pseudowollastonite	β-Cristobalite, α-quartz, β-quartz, wollastonite-1A	β-Cristobalite, α-quartz, β-quartz, wollastonite-1A	1000–1020°C
T_4	β-Quartz, β-cristobalite, α-quartz, Na_2CaSiO_4,	β-Cristobalite	β-Cristobalite	935–940°C

consistent with the primary phase field of wollastonite-2M as identified through room temperature XRD analysis of the devitrified C_3 glass. Further to this, we did not observe any sporadic or random crystallization, such as would be associated with severe alkali volatilization between the hot end of the boat and the liquidus temperature position of the C_3 glass. Furthermore, our observation that the alkali oxide content has an insignificant effect on the liquidus temperature, as indicated by our developed liquidus temperature models, further reduces alkali volatilization effects being a significant factor.

3.4 | High-temperature phase relations

3.4.1 | T-group glasses

Table 6 shows that high-temperature phase fields of the heat-treated T_1 glass at 800°C are α and β forms of quartz besides β-cristobalite. The forms of quartz are retained and the formation of Na_2CaSiO_4 is observed upon further heating to 900°C. On further heating Na_2CaSiO_4 decomposes, and α and β forms of quartz are retained as the main phase fields at about 1000°C. The α and β forms of quartz dissolve at around 1020°C which is significantly above the measured liquidus temperature of 965°C.

Tridymite, α and β forms of quartz, and β-cristobalite are the identified crystalline phases in heat-treated T_2 glass at 800°C. On further heating, tridymite disappears and β-cristobalite and α-quartz are retained at 900°C. Upon further heating the crystalline phase of β-cristobalite is preserved in the range of 985 to 1005°C, and finally, β-cristobalite dissolves when the temperature is raised to 1015°C which is markedly above the measured liquidus temperature of 947°C.

Devitrification products of the heat-treated T_3 glass are α and β forms of quartz, β-cristobalite, and pseudowollastonite at 800°C, and these crystalline phases are preserved when the temperature is raised to 900 and 1000°C. However, all devitrification products identified in T_3 glass dissolve when the temperature reaches to 1000°C which is far below the measured liquidus temperature of 1053°C.

Na_2CaSiO_4, α and β forms of quartz, and β-cristobalite are the main crystalline phases identified in heat-treated T_4 glass at 800°C. When the temperature is increased to 900°C, α and β forms of quartz and Na_2CaSiO_4 undergo decomposition; and β-cristobalite is retained. β-cristobalite is still preserved upon further heating of T_4 glass to 940°C. However, β-cristobalite disappears when the temperature of T_4 glass reaches 945°C which is slightly below the measured liquidus temperature of 961°C.

3.4.2 | C-group glasses

Table 7 shows that the heat treatment of C_1 glass at 800°C gives rise to crystalline phases of β-quartz, β-cristobalite, and tridymite-hexagonal. Upon further heating of C_1 glass to 900°C, crystalline phases of β-quartz and β-cristobalite dissolve and tridymite-hexagonal coexists with newly formed crystalline phases of Na_2CaSiO_4 and wollastonite-1A. When the heat treatment temperature is raised to the temperature range of 1050–1075°C, formation of α-cristobalite is identified and wollastonite-1A is retained as the other crystalline phases undergo decomposition. On further heating, all devitrification products of C_1 glass dissolve at 1075°C which is significantly above the measured liquidus temperature of 1025°C.

Heat treatment of C_2 glass at 800°C leads to the formation of crystalline phases of β-quartz, β-cristobalite, δ-Na_2SiO_5, and Na_2CaSiO_4. However, only β-quartz is preserved upon heating of C_2 glass to 900°C as the other devitrification products dissolve. α-quartz coexists with newly formed tridymite-2 h in the temperature range of 1010 and 1060°C, and both crystalline phases dissolve with further heating of C_2 glass to 1065°C which

TABLE 7 Identified crystalline phase fields of C-group glasses at 800 and 900°C and just below their HTXRD crystal dissolution points by in situ HTXRD analysis.

	Type of phase fields			
Glass Code	**800°C**	**900°C**	**Just below HTXRD crystal dissolution temperature**	
C_1	β-Quartz, β-cristobalite, tridymite—hexagonal	Na_2CaSiO_4, tridymite—hexagonal, wollastonite 1A	α-Cristobalite, wollastonite 1A	1050–1075°C
C_2	β-Quartz, β-cristobalite, δ-Na_2SiO_5, Na_2CaSiO_4	β-Quartz	**α-Quartz**, tridymite −2H	1010–1060°C
C_3	β-Quartz, α-quartz, Na_2CaSiO_4	β-Cristobalite, β-quartz, **α-quartz**	Unknown	1100°C
C_4	Pseudowollastonite, α-quartz	α-Quartz, pseudowollastonite, β-cristobalite, $Na_2Ca_2Si_3O_9$	α-Cristobalite	1045–1050°C
C_5	β-Quartz, Na_2CaSiO_4, β-cristobalite, α-quartz	β-Quartz, Na_2CaSiO_4, β-cristobalite, α-quartz	β-Cristobalite	1025°C
C_6	β-Quartz, Na_2CaSiO_4	β-Cristobalite, α-quartz	β-Cristobalite	970°C

Note: Crystalline phase field of quartz that is shown in bold is deemed to be α-quartz according to the work of Martínez et al.[45]

is slightly below the measured liquidus temperature of 1049°C.

Na_2CaSiO_4 and α and β forms of quartz are the main crystalline phases identified in heat treated C_3 glass at 800°C. Crystalline phases of α and β forms of quartz are retained whilst Na_2CaSiO_4 undergoes decomposition and formation of β-cristobalite is observed with increasing heat-treatment temperature to 900°C. However, identified crystalline phases of C_3 glass at 900°C disappear, and formation of an unknown crystalline phase is observed when the heat-treatment temperature is increased above 1070°C, and the X-ray amorphous phase is obtained upon further heating of devitrified C_3 glass to 1105°C which is significantly above the measured liquidus temperature of 1063°C.

Devitrification products of C_4 glass at 800°C are pseudowollastonite and α-quartz. Pseudowollastonite and α-quartz are retained, and crystalline phases of cristobalite and $Na_2Ca_2Si_3O_9$ form upon heating of C_4 glass to 900°C. However, these identified crystalline phases dissolve except α-cristobalite when the heat-treatment temperature is raised to 1045°C. Finally, α-cristobalite disappears and the X-ray amorphous phase of C_4 sample is obtained when the temperature reaches to 1060°C which is above the measured liquidus temperature of 1032°C.

Na_2CaSiO_4, α and β forms of quartz and β-cristobalite are the main crystalline phases of devitrified C_5 glass at 800°C, and these phase fields are retained further upon increasing the temperature to 900°C. On further heating, all devitrification products dissolve except β-cristobalite at 1025°C. Finally, β-cristobalite dissolves and the X-ray amorphous phase of C_5 is obtained when the temperature reaches 1030°C which is below the measured liquidus temperature of 1057°C.

Following the devitrification process at 800°C, formation of β-quartz and Na_2CaSiO_4 is observed in C_6 glass. Upon further heating, these crystal phases disappear and the formation of α-quartz and β-cristobalite is observed at 900°C. When the temperature is raised to 970°C, α-quartz dissolves but β-cristobalite is preserved. However, β-cristobalite disappears upon further heating of C_6 glass to 980°C which is slightly below the measured liquidus temperature of 1020°C.

3.4.3 | Effect of alkali volatilization on the HTXRD crystalline phase fields

In our HTXRD experiments, the primary heat treatment stages at 800 and 900°C last for about ∼30 h, which is slightly longer than the typical 24-h residence time used in the standard gradient method for measuring liquidus temperature.[7,10] Furthermore, the heat treatment temperatures of 800 and 900°C used in this experiment are significantly lower than the temperatures typically employed for standard liquidus temperature measurements in commercial soda–lime–silica glasses.[7,9,10] This suggests that the likely extent of alkali volatilization at the heat treatment temperatures of 800 and 900°C will be comparable to that which occurs during standard liquidus temperature measurements. Devitrified melts of the studied glasses became almost entirely X-ray amorphous within the temperature range of 945 to 1105°C after a maximum of 15 h of heat treatment, which occurred after the heat treatment stage at 900°C. Hence, it is anticipated that a higher degree of alkali volatilization for the devitrified glasses would occur at heat treatment temperatures between 900 and 1105°C.

TABLE 8 The measured liquidus temperatures by gradient boat method and HTXRD dissolution point of devitrification phases for the studied glasses.

Glass code	Measured T_L/°C	T_{HT}/°C	ΔT/°C
T_1	965	1020	55
T_2	947	1015	68
T_3	1053	1000	−53
T_4	961	945	−16
C_1	1025	1075	50
C_2	1049	1065	16
C_3	1063	1105	42
C_4	1032	1060	28
C_5	1057	1030	−27
C_6	1020	980	−40

Note: A maximum variation of ±14.14°C would be estimated for (T_L-T_{HT}). The error in ΔT can be calculated by using $\delta\Delta T = \sqrt{(\Delta T_{T_L})^2 + (\Delta T_{HT})^2}$ where ΔT_{T_L} and ΔT_{HT} are ±20 and ±10°C, respectively. $\delta\Delta T$ = 22.36°C.

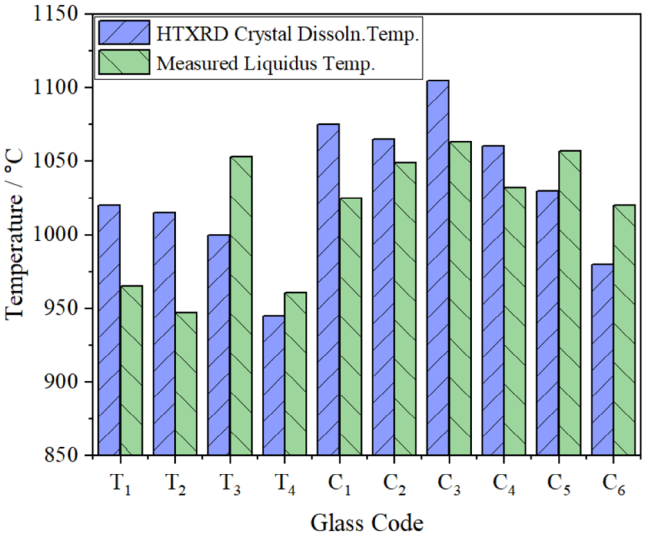

FIGURE 3 Measured liquidus and HTXRD crystal dissolution temperatures of the studied T- and C-group glasses.

CaO is one of the major oxides of the studied glasses and can play a notable effect on the type of crystal formation in soda–lime–silica glasses. In the case of significant alkali volatilization, the relative concentration of CaO could notably increase and would significantly influence the type of crystal formation.[41] This effect may manifest as a shift toward different wollastonite polymorphs within the studied compositional range of the soda–lime–silica glass melts. However, the HTXRD patterns obtained during the 30 × 30 min scans at 800 and 900°C show no such behavior and do not support the hypothesis of any noticeable shift in the primary phase fields to wollastonite polymorphs that could be associated with alkali volatilization. The formation of wollastonite is indeed observed during the heat treatment stages, but it occurs intermittently and coexists with other phase fields (see Tables 6 and 7. In contrast, SiO_2 crystalline phases are consistently prevalent throughout all heat treatment stages and at the crystal dissolution positions of the HTXRD experiment.

3.4.4 | Measured T_L versus T_{HT}

Devitrified glasses that were subjected to heat treatment were slowly heated at a rate of 1°C/min from 900 to 1200°C to determine the dissolution point of last crystal (T_{HT}) prior to formation of X-ray amorphous melt. Dissolution of crystalline phases in glass melts, in theory, is expected upon heating of devitrified glasses to marginally above their measured liquidus temperatures. However, the dissolution of SiO_2 polymorphs in T_1, T_2, C_1, C_2, C_3, and C_4 glasses occurs at much higher temperatures than their actual liquidus temperatures (Table 8 and Figure 3). Note that microscopic examination cannot identify very small crystals that exist beyond the visible actual liquidus temperature position, but such very small crystals can be X-ray detectable, and hence it is reasonable to observe such crystal structures markedly above their microscopic liquidus temperature by X-ray diffraction analysis. On the other hand, the literature reported that tridymite and cristobalite crystals redissolve very slowly despite the glass melt temperature is raised substantially above its liquidus temperature.[9] Hence, the formation of tridymite is particularly avoided in float glass melts as a critical processing requirement.[43] HTXRD analysis of the studied glasses shows that tridymite is a rarely observed crystalline phase field in commercial soda–lime–silica glass melts. Our results and literature data suggest that the rate of dissolution of these metastable SiO_2 phases might be sensitive to the residence time of melts above their liquidus temperatures, and therefore a heating rate of 1°C/min may not be sufficiently slow to readily dissolve the crystals near their corresponding liquidus temperatures.

As was noted above, metastable SiO_2 polymorphs might be also resistant to dissolution irrespective of applied heating rates. On the contrary, SiO_2 polymorphs which formed in T_3, T_4, C_5, and C_6 glasses redissolve at lower temperatures than their measured liquidus temperatures (Table 8 and Figure 3). One of the co-authors[44] of this study previously established the deviation of thermocouple temperature from actual Anton Paar HTK1200N hot stage temperature and was less than ±10°C. The cumulative error in measured liquidus temperature by gradient boat method for the studied glasses, including other systematic errors, was conservatively estimated to be ±20°C. Hence, delta temperatures between liquidus and hot-stage crystal dissolution positions greater than ±22.36°C (see

Table 8) can be regarded as significant. Consequently, the dissolution of SiO_2 polymorphs in only T_3 and C_6 glasses below their liquidus temperatures can be regarded as statistically significant; and such lower crystal dissolution temperatures than their liquidus temperatures cannot be attributed to the variation of glass composition or the type of phase fields.

One potential reason for the significantly greater value of the measured liquidus temperature compared with the HTXRD crystal dissolution temperature for T_3 and C_6 glasses is that the actual liquidus temperatures may be lower than the measured values. However, T_3 glass contains one of the highest concentrations of CaO among T- and C-group glasses, and the dominant role of CaO in increasing liquidus temperature is previously noted in Section 3.3. Hence, the high CaO concentration in T_3 glass is a plausible explanation for the relatively higher measured liquidus temperature. In the case of C_6 glass, it exhibits one of the lowest measured liquidus temperatures among the C-group glasses, and it appears that the measured liquidus temperature is consistent with the glass composition and there is no indication that the actual liquidus temperature would be significantly different from its measured value. On the other hand, the applied heating rate may be too fast and may not have allowed sufficient time for phase equilibrium to be established, especially after the transient solid phases have disappeared at the HTXRD crystal dissolution temperature, and therefore, the measured liquidus temperature may indeed appear higher than the HTXRD crystal dissolution temperature.

3.4.5 | Variation of T_{HT} with glass composition

We also explored the associations between composition and HTXRD crystal dissolution temperature of glasses by multiple linear regression analysis. The result indicated that *p*-values of all glass oxides become statistically insignificant (>.05) when combination of SiO_2, CaO, MgO, Al_2O_3, K_2O, Cr_2O_3, and Fe_2O_3 are added as predictive variables. Whereas Na_2O or Fe_2O_3 become statistically significant ($p < .05$) when they are added as a single predictive variable into the simple linear regression analysis. However, the results also show that neither simple nor multiple regression analysis has been able to establish a strong association between the glass composition and the HTXRD crystal dissolution temperature. Nevertheless, regression analysis has yielded the highest R^2 value of ~0.60 for the simple regression model when using Fe_2O_3 alone as the predictive variable. When both Na_2O and Fe_2O_3 are included as predictive variables in the model, the R^2 value increases to approximately 0.71, showing an improvement in the model's goodness of fit, and a higher Na_2O content was correlated with lower crystal dissolution temperature. Note that the simple model also indicates that the presence of Cr_2O_3 does not have a significant effect on the HTXRD crystal dissolution temperature of the studied glasses. Conversely, Hrma et al.[21] reported that the addition of 1 mol % Cr_2O_3 in place of SiO_2 increases liquidus temperature of nuclear waste glasses by 100°C, but the increase was much less for Fe_2O_3. Note that the notable impact of Fe_2O_3 or Cr_2O_3 on the crystallization properties was reported within the spinel (i.e., hematite, magnetite, or chromite) primary phase field of high iron and/or chromium oxide-containing glasses.[21] However, the Fe_2O_3 levels in our highest iron oxide containing glasses are still significantly lower than those found in glasses where the primary phase field is spinel, and the HTXRD patterns do not indicate any evidence of formation of spinel crystalline phases across the range of heat treatment temperatures. On the other hand, significantly higher crystal dissolution temperatures can be observed for the C_1, C_2, C_3, and C_4 glasses (Figure 3), which have the highest Fe_2O_3 and Cr_2O_3 concentrations among the studied T- and C-group glasses. On the contrary, T_1 and T_2 glasses, which have measurably low Fe_2O_3 levels also have higher crystal dissolution temperatures relative to their liquidus temperatures, nonetheless the crystal dissolution temperature for T_1 and T_2 did not reach the levels observed in the C-group glasses. Despite the discrepancy in results between T- and C-group glasses, the correlation between HTXRD crystal dissolution temperature with Fe_2O_3 and Na_2O contents, as indicated by the R^2 value of 0.71, remains noteworthy givin the complex nature of HTXRD experiments.

3.4.6 | Unassigned high temperature SiO_2 and unknown crystalline phases

In addition to the assigned crystalline phases from HTXRD patterns of T- and C-group glasses, sporadic unknown crystalline phase was also detected from X-ray diffraction patterns of T_1, T_2, T_3, C_1, C_2, and C_3 glasses obtained at various temperatures between 900 and 1100°C. It appears that the relationship between unknown crystalline phase formation and chemical composition is not clear-cut as the total alkali, alkaline-earth, and network-former oxide concentrations of these glasses significantly vary from each other. Hence, existence of unknown crystalline phase cannot be attributed to the concentration or presence of any specific oxides in these glasses. Figure 4 is a representative of the HTXRD patterns of the studied glasses and demonstrates the assigned and unknown crystalline phases of C_3 glass at various temperatures between 1010 and 1100°C. Figure 5 demonstrates the characteristic Bragg diffraction

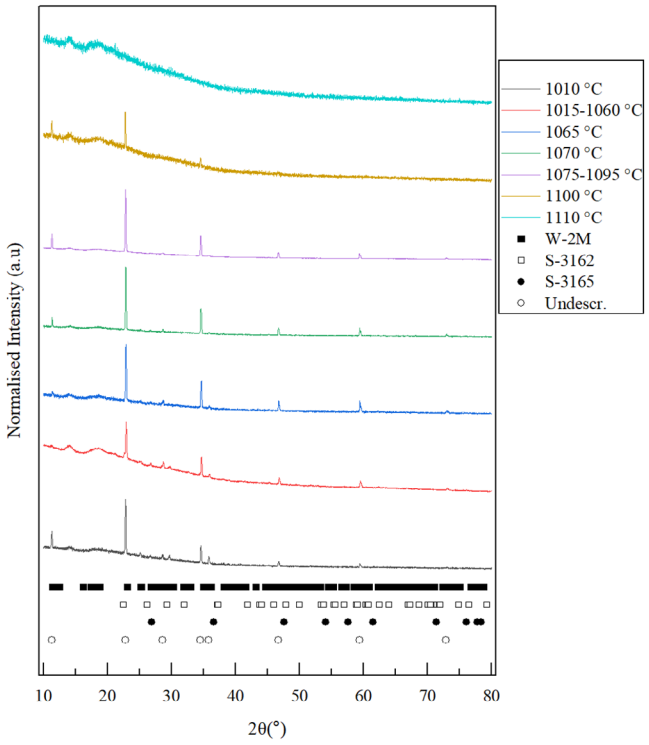

FIGURE 4 Representative in situ high-temperature X-ray diffraction patterns of devitrified C_3 glass melt at various heat-treatment temperatures. Cluster analysis has been adopted for the data between 1015–1060°C and 1075–1095°C, and their most representative scans were presented for the corresponding temperature ranges. S-3162 and S-3165 stand for high-temperature SiO_2 polymorphs of PDF # 01–075 3162 and 01–075 3165, respectively. *Undescr.* denotes the 2θ (°) positions of the strongest Bragg diffraction peaks of high temperature unknown primitive-cubic crystalline phase.

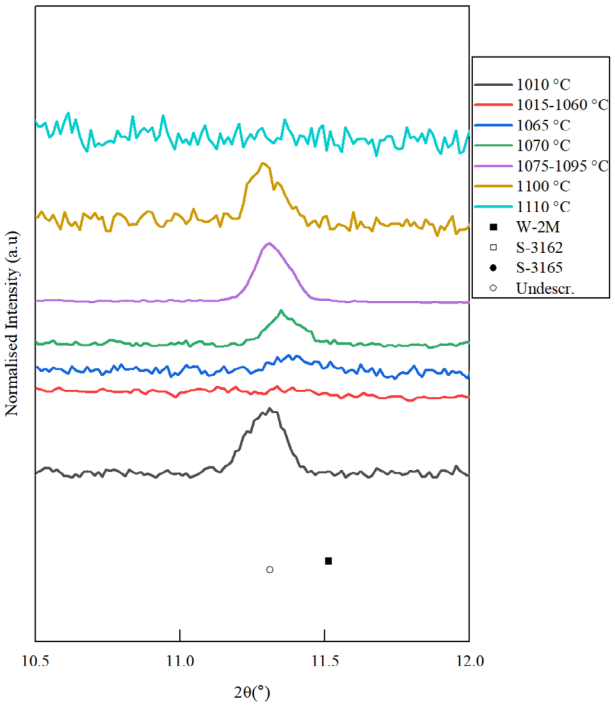

FIGURE 5 Representative in situ high-temperature X-ray diffraction patterns of devitrified C_3 glass at various heat-treatment temperatures over the range 10.5–12 2θ (°).

peak of unknown primitive-cubic crystalline phase positioned at 11.32° 2θ, and this peak does not belong to the diffraction patterns or powder diffraction files of the other types of crystalline phases that are identified in studied glasses. The unknown crystalline phase that existed at 1010°C disappears up to 1065°C. Upon further heating, this unknown crystalline phase appears again following the dissolution of wollastonite-1A and remains the final primary phase field up to 1100°C prior to formation of the X-ray amorphous phase at 1115°C. Further to these, tetragonal and hexagonal structured high-temperature SiO_2 polymorphs (PDF # 01–075 3162 and 01–075 3165) that exhibit distinct X-ray diffraction patterns to traditional SiO_2 polymorphs (quartz, cristobalite, and tridymite) are the frequently observed crystalline structures in devitrified T- and C-group glasses. These high-temperature SiO_2 polymorphs previously identified[45] in partially crystallized sol-gel derived amorphous SiO_2, and their X-ray diffraction patterns have led to suggestion that these high-temperature SiO_2 phases resemble quartz. Hence, these high temperature SiO_2 phases that were observed in devitrified T- and C-group glass melts are deemed to be α-quartz. Further to these, room temperature X-ray diffraction pattern of air-quenched C_3 glass which was devitrified at 30°C below its actual liquidus temperature does not indicate any traces of unknown or high-temperature SiO_2 polymorphs but reveals existence of wollastonite-2M. This suggests that the crystalline phases which were identified from in situ high-temperature X-ray diffraction studies are only high-temperature-specific phases and are not recoverable at room temperature.

3.4.7 | Comparison of high-temperature phase relations with literature

It is known that α-quartz undergoes phase transformation to β-quartz at around 573°C in a pure SiO_2 system.[46] Morey[40] also observed quartz as a primary crystalline phase in rapidly cooled SiO_2–Na_2O–CaO ternary glasses with >74 mass % SiO_2 and > 20 mass % Na_2O. However, literature data does not report the formation of quartz in quinary commercial soda–lime–silica glasses upon rapid cooling. On the contrary, our in situ high-temperature X-ray diffraction study indicates that α and β forms quartz can be identified in quinary commercial soda–lime–silica glass melts from 800 to up to 1060°C as was observed in T- and C-group glasses. Tables 6 and 7 show that sporadic pseudowollastonite, β-cristobalite, tridymite, and binary/ternary Na_2O–CaO–SiO_2 solid compounds

(Na_2CaSiO_4, δ-Na_2SiO_5, $Na_2Ca_2Si_3O_9$) are the identified crystalline phases at 800°C. Note that these binary/ternary phases may only crystallize from very pure Na_2O–CaO–SiO_2 melts, and are rarely observed in rapidly-cooled devitrified commercial soda–lime–silica glasses, rather metastable substitutes of devitrite or β-wollastonite forms in quinary commercial silicate glass melts.[15,47] This suggests that high temperature stable Na_2CaSiO_4, δ-Na_2SiO_5, and $Na_2Ca_2Si_3O_9$ solid phases may transform into metastable crystal form of wollastonite or devitrite upon rapid-cooling in quinary soda–lime–silica glasses. On the other hand, α and β forms of quartz are the most abundant high-temperature crystalline phases in most heat-treated T- and C-group glasses at 800°C. Although α and β forms of quartz still retained the major crystalline phase fields upon increasing heat treatment temperature to 900°C, the relative abundance of other crystalline phases such as different polymorphs of SiO_2, wollastonite and binary/ternary Na_2O–CaO–SiO_2 solid compounds also increases.

The work of Hrma et al.[7] investigated the crystallization properties of different float-like glasses quenched from heat treatment temperature of 900°C and did not observe any forms of quartz or binary/ternary solid Na_2O–CaO–SiO_2 compounds in those glasses. On the other hand, they identified devitrite and cristobalite as the major crystalline phases which were in equilibrium with lower fractions of wollastonite and tridymite. Similarly, our previous room temperature X-ray diffraction study[11] revealed that wollastonite polymorphs were the dominant primary crystalline phase field for most soda–lime–silica glasses that were rapidly cooled down from their liquidus temperatures positions, and the type of crystalline phase did not vary significantly with composition when considered against the wide range of compositional modifications. Our HTXRD study therefore indicates that α and β forms of quartz, Na_2CaSiO_4, δ-Na_2SiO_5, and $Na_2Ca_2Si_3O_9$ can be regarded as the high temperature—stable or specific crystalline solid phases and are not recoverable at room temperature as these crystalline phases are not traditionally observed in room temperature X-ray diffraction studies. It is possible that these crystalline phases either transform into other metastable crystalline phases or undergo decomposition upon rapid cooling of silicate glass melts. Note that when the heat treatment temperature of studied glasses is further increased to slightly below their actual HTXRD crystal dissolution temperatures, binary/ternary phase fields of Na_2CaSiO_4, δ-Na_2SiO_5, and $Na_2Ca_2Si_3O_9$ redissolve in all T- and C-group glass melts as the other existing phase fields of tridymite, cristobalite wollastonite, and quartz are preserved.

Bartuska[48] reported that the formation of cristobalite occurs at relatively low temperatures in industrial glasses. However, these forms of cristobalite occur in all heat treatment stages irrespective of the heat treatment temperatures, but we were unable to determine whether cristobalite is in the form of a primary phase or in trace amounts alongside other crystalline phases at the heat treatment stages of 800 and 900°C. Nevertheless, it can be clearly seen from Tables 6 and 7 that α and β forms of cristobalite become the primary and sole crystalline phase in most studied glasses here prior to formation of X-ray amorphous melt near HTXRD crystal dissolution temperature. This agrees with the work of Hrma et al.[7] in which they found that SiO_2 is the major crystalline phase slightly below liquidus temperature of float-type glasses, but they were uncertain whether the silica primary phase in those glasses is tridymite or cristobalite. Whereas Beerkens and Conradt[15] frequently observed pseudowollastonite as a primary phase field in devitrified industrially manufactured float glasses that were rapidly cooled from their liquidus temperature positions. Beerkens and Conradt[15] and Hrma et al.[7] reported that the maximum temperature for SiO_2 crystallization increases with increasing SiO_2 levels in glass. However, cristobalite polymorphs were the primary phase field for most studied glasses just below their crystal dissolution temperature even though their silica concentrations significantly vary from each other. This suggests that there is no clear relationship between the maximum temperature of SiO_2 crystallization and silica concentration.

3.4.8 | Effect of HTXRD phase fields on gradient method liquidus temperature

As discussed in Section 3.4.7, the metastable crystalline form of wollastonite polymorphs, devitrite, and different SiO_2 phases are the primary phase fields that are present at the liquidus temperature positions of quenched commercial soda–lime–silica glasses. However, specific binary/ternary Na_2O–CaO–SiO_2 solid compounds, such as Na_2CaSiO_4, δ-Na_2SiO_5, $Na_2Ca_2Si_3O_9$, along with polymorphs of quartz and β-cristobalite, which are not typically observed in quenched devitrified melts of soda–lime–silica glasses, become the most prevalent crystalline phases at high temperatures. This implies that the observations made during the HTXRD experiments likely represent behavior at temperatures close to the liquidus temperatures of the studied glasses during the gradient method liquidus temperature experiments. During the gradient method liquidus temperature experiments, these high temperature stable and specific binary/ternary Na_2O–CaO–SiO_2 solid compounds, as well as β-quartz and β-cristobalite which are expected to be present, may undergo dissolution or transformation into more stable crystal structures at lower temperatures as the glass cools. Consequently, this scenario suggests that the high-temperature stable crystalline phases at the liquidus

temperature position may dissolve, or the liquidus temperature position may shift to lower temperatures due to the formation of lower-temperature stable crystalline phases upon cooling. This indicates that the liquidus temperatures of the quenched soda–lime–silica glasses within the gradient boat may appear lower than those observed at high temperatures.

4 | CONCLUSION

Most of the investigated glass compositions, particularly of those T-group glasses resemble closely that of commercial float glasses. Hence, results obtained for T-group glasses may also represent the crystallization and working properties of float-type glasses. The multiple variable regression analysis suggests that CaO is the predictive variable that is associated with the greatest increase in liquidus temperature. Therefore, it can be concluded that T-group glasses which have significantly low levels of CaO exhibit lower liquidus temperatures compared with the high-CaO-containing C-group glasses. It is therefore the delta between glass melt processing and liquidus temperatures appears to be very large for industrially manufactured low-CaO-containing soda–lime–silica glasses, particularly for T-group glasses. Reformulation of commercial float, container, and domestic soda–lime–silica glass compositions for delta temperature minimization could be realized for improving melting and refining properties of commercial silicate glasses.

Crystallization properties of soda–lime–silica glasses obtained from room and high-temperature X-ray diffraction studies can significantly differ from each other. Different forms of quartz, Na_2CaSiO_4, δ-Na_2SiO_5, and $Na_2Ca_2Si_3O_9$ are the frequently observed crystalline phases in devitrified soda–lime–silica glass melts at temperatures between 900 and 1000°C. However, the literature does not report the formation of these crystal phases in rapidly cooled soda–lime–silica glasses. This suggests that these phase fields may transform into metastable substitutes of devitrite and wollastonite upon rapid cooling. High-temperature X-ray diffraction analysis also indicated that cristobalite polymorphs are the primary crystalline phases in most cases prior to formation of X-ray amorphous melts irrespective of glass composition or silica concentration. On the contrary, pseudowollastonite and devitrite are found to be the primary phase fields for the devitrified commercial soda–lime–silica glasses that are rapidly cooled from their liquidus temperature positions. Sporadic and irrecoverable high-temperature unknown primitive-cubic or quartz-like SiO_2 phases, which are also identified from HTXRD patterns, may influence the actual liquidus temperature of silicate glass melts. Overall, cristobalite polymorphs, high-temperature SiO_2, and unknown crystal phases that form at realistic glass processing temperatures should play a key role in determining the high liquidus temperature and therefore workability of commercial soda–lime–silica glasses.

ACKNOWLEDGEMENTS

The authors have nothing to report.

FUNDING INFORMATION

None.

ORCID

Erhan Kilinc https://orcid.org/0000-0002-5280-0275
Paul A. Bingham https://orcid.org/0000-0001-6017-0798

REFERENCES

1. Wallenberger FT, Bingham PA. Fiberglass and glass technology: energy-friendly compositions and applications. Springer; 2010.
2. Smrcek A. Evolution of the compositions of commercial glasses 1830 to 1990. Part II. Container glass. Glass Sci Technol (Frankfurt). 2005;78(5):230–44.
3. Stadler LE, Cronin D. Container glass composition: I. Glass industry. 1977;58(12):10–14.
4. Sonne CR, Lester WR. Container glass compositions 1932 to 1960. Glass Ind. 1965;623:134–37.
5. Weigand R, Hessenkemper H, Rossel AK, Tritschel D, Hubner L, Mai F. Potential for savings in the container glass industry. Interceram. 2012;(63):410–13.
6. Sinton CW, LaCourse WC. Experimental survey of the chemical durability of commercial soda-lime-silicate glasses. Mat Res Bull. 2001;36(13-14):2471–79.
7. Hrma P, Smith DE, Matyáš J, Yeager JD, Jones JV, Boulos EN. Effect of float glass composition on liquidus temperature and devitrification behaviour. Phys Chem Glas: Eur J Glass Sci Technol B. 2006;47(1):64–76.
8. Silverman WB. Effect of alumina on devitrification of sodium oxide-dolomite lime-silica glasses. J Am Ceram Soc. 1940;23(9):274–81.
9. Wallenberger FT, Smrček A. The liquidus temperature; its critical role in glass manufacturing. Int J Appl Glass Sci. 2010;1(2):151–63.
10. Bingham PA, Marshall M. Reformulation of container glasses for environmental benefit through lower melting temperatures. Glass Technol. 2005;46(1):11–19.
11. Kilinc E, Bell AM, Bingham PA, Hand RJ. Effects of composition and phase relations on mechanical properties and crystallization of silicate glasses. J Am Ceram Soc. 2021;104(8):3921–46.
12. Karlsson KH, Backman R, Hupa L. Models for liquidus temperatures. In Proceedings of the VI European Glass Society Conference. Montpellier. [Internet]. 2002. [2023 Nov 2]. Available from: http://kdsolution.com/pdfupload/Karlsson.pdf
13. Swift HR. Effect of magnesia and alumina on rate of crystal growth in some soda-lime-silica glasses. J Am Ceram Soc. 1947;30(6):170–74.
14. Silverman WB. Effect of alumina on devitrification of soda-lime-silica glasses. J Am Ceram Soc. 1939;22(1-12):378–84.
15. Beerkens RG, Conradt R. Round robin test on liquidus temperature of soda–lime–magnesia–silica float glass samples: a technical report of the ICG Technical Committee (TC 18) on

properties of glass forming melts. Glass Technol: Eur J Glass Sci Technol A. 2008;49(5):205–12.
16. Fluegel A. Modeling of glass liquidus temperatures using disconnected peak functions. InACerS 2007 glass and optical materials division meeting. http://glassproperties.com/liquidus 2007.
17. Cuartas R. Calculo teorico de propiedades del vidrio: viscosidad, parametros termicos y parametros de desvitrificacion. Ceramica et Vidrio. 1984;23:105–11.
18. Fluegel A. Glass viscosity calculation based on a global statistical modelling approach. Glass Technol: Eur J Glass Sci Technol A. 2007;48(1):13–30.
19. Bell AM, Backhouse DJ, Deng W, Eales JD, Kilinc E, Love K, et al. X-ray fluorescence analysis of feldspars and silicate glass: effects of melting time on fused bead consistency and volatilisation. Minerals. 2020;10(5):442.
20. Grauer OH, Hamilton EH. Improved apparatus for determination of liquidus temperatures and rates of crystal growth in glasses. J Res Natl Bur Stand. 1950;44(5):495–502.
21. Hrma PR, Vienna JD, Mika M, Crum JV, Piepel GF. Liquidus temperature data for DWPF glass. Report No: PNNL-11790. Pacific Northwest National Laboratory. [Internet]. 1998. [2023 Nov 2]. Available from: https://www.pnnl.gov/main/publications/external/technical_reports/PNNL-11790.pdf
22. Mauro JC, Yue Y, Ellison AJ, Gupta PK, Allan DC. Viscosity of glass-forming liquids. Proc Natl Acad Sci. 2009;106(47):19780–84.
23. Ferkl P, Hrma P, Kruger AA. Augmented Adam-Gibbs model for glass melt viscosity and configuration entropy as functions of temperature and composition. J Non-Cryst Solids. 2022;595:121832.
24. Neuville DR. Viscosity, structure and mixing in (Ca, Na) silicate melts. Chem Geol. 2006;229(1-3):28–41.
25. Hrma P. High-temperature viscosity of commercial glasses. Ceramics Silikaty. 2006;50(2):57.
26. Biavati A. Correlation between manufacturing defects and workability parameters of soda-lime glass. Int Glass J (Testo stampato). 2004;130(130):14–17.
27. Hessenkemper H, Brückner R. Some aspects of the workability of glass melts. Glastechnische Berichte. 1990, 63(2):19–23.
28. McGraw DA. Transfer of heat in glass during forming. J Am Ceram Soc. 1961;44(7):353–63.
29. Manring WH, Diken GM. A practical approach to evaluating redox phenomena involved in the melting-fining of soda-lime glasses. J Non-Cryst Solids. 1980;38:813–18.
30. CRB Analyse Service GmbH [Internet] Bahnhofstraße 14 //37181 Hardegsen (Germany) [Reviewed 2023 Sep 01; cited 2023 Sep 28] Available from: https://www.crb-gmbh.com/en/analysis/xray-fluorescence/glass#oben
31. Yilmaz SG. Okcular. (Bigadic-Balikesir) Perlit Yataklari ve Perlitin Cam Endustrisinde Kullanimi [Dissertation on the Internet]. 2001. [2023 Nov 2]. Istanbul Technical University. Available from: https://polen.itu.edu.tr/items/bb767f4b-23cf-4854-875e-16b3b5a474f8
32. Bingham K. Low soda glass development. In: 42nd Conference on glass problems. John Wiley & Sons; 2009. 3(3/4): p. 186.
33. Williams HP. The Influence of chemical composition on the working properties of container glass. Glasteknisk Tidskrift. 1982;37(3):77–82.
34. Weigand R, Hessenkemper H, Rossel AK, Tritschel D, Hubner L, Mai F. Potential for savings in the container glass industry. Interceram Refractories. 2011;63(410-413):28–32.
35. Xiao Z, Cheng J, Wu H. Effect of Al_2O_3/SiO_2 ratio on the viscosity and workability of high-alumina soda-lime-silicate glasses. J Chin Ceram Soc. 2012;40(7):1000–1005.
36. Li L, Han J, Lin HJ, Ruan J, Wang J, Zhao X. Simulation of glass furnace with increased production by increasing fuel supply and introducing electric boosting. Int J Appl Glass Sci. 2020;11(1):170–84.
37. Dreyfus C, Dreyfus G. A machine learning approach to the estimation of the liquidus temperature of glass-forming oxide blends. J Non-Cryst Solids. 2003;318(1-2):63–78.
38. Contribution of the Owens-Illinois Glass Company General Research Laboratory. Effect of boric oxide on properties of soda-dolomitic lime-silica glass. J Am Ceram Soc. 1948;31(1):8–14.
39. Owens-Illinois Glass Company General Research Laboratory. Effect of substituting MgO for CaO on properties of typical soda-lime glasses. J Am Ceram Soc. 1944;27(8):221–25.
40. Morey GW. The devitrification of soda-lime-silica glasses1. J Am Ceram Soc. 1930;13(10):683–713.
41. van Limpt JA. Modelling of evaporation processes in glass melting furnaces. [Dissertation on the Internet]. 2007. [2023 Nov 2]. Eindhoven University of Technology. Available from: https://research.tue.nl/files/3207578/200702749.pdf
42. Beerkens RG. Modelling the kinetics of volatilization from glass melts. J Am Ceram Soc. 2001;84(9):1952–60.
43. Hrma PR, Smith DE, Yeager JD, Lam OP. Thermochemical optimization of float glass composition: low-alumina glass development. Report No: PNNL-13958. Pacific Northwest National Laboratory. [Internet]. 2002. [2023 Nov 2]. Available from: https://www.pnnl.gov/main/publications/external/technical_reports/PNNL-13958.pdf
44. Bell AM. Orthorhombic-cubic phase transition in $Rb_2CoSi_5O_{12}$ leucite analogue. Minerals. 2023;13(2):210.
45. Martínez JR, Palomares-Sánchez S, Ortega-Zarzosa G, Ruiz F, Chumakov Y. Rietveld refinement of amorphous SiO_2 prepared via sol–gel method. Mater Lett. 2006;60(29-30):3526–29.
46. Ohno I, Harada K, Yoshitomi C. Temperature variation of elastic constants of quartz across the α-β transition. Phys Chem Miner. 2006;33:1–9.
47. Zhang Z, Xiao Y, Voncken J, Yang Y, Boom R, Wang N, et al. Phase equilibria in the Na_2O–CaO–SiO_2 system. J Am Ceram Soc. 2011;94(9):3088–93.
48. Bartuška M. Crystalline inclusions. In: Glass flaws (in Czech). Prah (Praha), 2001.

How to cite this article: Kilinc E, Bell AMT, Bingham PA. Dynamic high-temperature crystallization and processing properties of industrial soda–lime–silica glasses. J Am Ceram Soc. 2023;1–18. https://doi.org/10.1111/jace.19602